Biochimica et Biophysica Acta 1788 (2009) 2142–2149

Contents lists available at ScienceDirect

Biochimica et Biophysica Acta

journal homepage: www.elsevier.com/locate/bbamem

Lipid domains in giant unilamellar vesicles and their correspondence with equilibrium thermodynamic phases: A quantitative fluorescence microscopy imaging approach

M. Fidorra [a,b,c,1], A. Garcia [d,1], J.H. Ipsen [b,c], S. Härtel [d,*], L.A. Bagatolli [a,b,*]

[a] Membrane Biophysics and Biophotonics group /Department of Biochemistry and Molecular Biology, University of Southern Denmark, Campusvej 55, Dk-5230 Odense M, Denmark
[b] MEMPHYS, Center for Biomembrane Physics, University of Southern Denmark, Campusvej 55, Dk-5230 Odense M, Denmark
[c] Department of Physics and Chemistry, University of Southern Denmark, Campusvej 55, Dk-5230 Odense M, Denmark
[d] Laboratory for Scientific Image Processing (SCIAN-Lab), Anatomy and Developmental Biology Program, Faculty of Medicine, University of Chile, Santiago, Chile and Nucleus of Neural Morphogenesis (NEMO), Santiago, Chile

ARTICLE INFO

Article history:
Received 16 June 2009
Received in revised form 27 July 2009
Accepted 7 August 2009
Available online 21 August 2009

Keywords:
Lipid domain
Giant unilamellar vesicle
Equilibrium thermodynamic phase
Confocal fluorescence microscopy
Lever rule
3D reconstruction

ABSTRACT

We report a novel analytical procedure to measure the surface areas of coexisting lipid domains in giant unilamellar vesicles (GUVs) based on image processing of 3D fluorescence microscopy data. The procedure involves the segmentation of lipid domains from fluorescent image stacks and reconstruction of 3D domain morphology using active surface models. This method permits the reconstruction of the spherical surface of GUVs and determination of the area fractions of coexisting lipid domains at the level of single vesicles. Obtaining area fractions enables the scrutiny of the lever rule along lipid phase diagram's tie lines and to test whether or not the coexistence of lipid domains in GUVs correspond to equilibrium thermodynamic phases. The analysis was applied to DLPC/DPPC GUVs displaying coexistence of lipid domains. Our results confirm the lever rule, demonstrating that the observed membrane domains correspond to equilibrium thermodynamic phases (i.e., solid ordered and liquid disordered phases). In addition, the fact that the lever rule is validated from 11 to 14 randomly selected GUVs per molar fraction indicates homogeneity in the lipid composition among the explored GUV populations. In conclusion, our study shows that GUVs are reliable model systems to perform equilibrium thermodynamic studies of membranes.

1. Introduction

Since the late 1990s, giant unilamellar vesicles (GUVs) have been extensively used as a model system to study phase coexistence in membranes. The average size of this model system (mean diameter ~25 μm) is considerably larger than the intrinsic resolution limit of light microscopy (~250 nm), allowing observation of particular membrane structural details at the level of single vesicles. This particular type of spatial information at the level of single liposomes is not directly accessible by experimental approaches such as differential scanning calorimetry, fluorescence spectroscopy, X-ray diffraction, FTIR, EPR, or NMR, where "bulk" mean parameters are measured using solutions of liposomes (multilamellar vesicles, small or large unilamellar vesicles). In addition, the mean size of GUVs is comparable to that of cellular plasma membranes, which makes GUVs a suitable model system to determine the diverse properties of this important biological constituent.

The first studies of the lateral membrane scenario on GUVs using fluorescence microscopy related techniques were published almost a decade ago [1–6]. These studies reported on the direct visualization of micrometer-sized lipid domains in single GUVs composed of different lipid mixtures at relevant compositions and temperatures. In these experiments, the local physical properties of the observed lipid domains (measured using either dipolar relaxation [1–3] or diffusion [5] of particular fluorophores) were used to associate presence of lipid domains with equilibrium thermodynamic phases.

At present, the most common approach used to correlate the presence of lipid domains with thermodynamic phases in GUVs relies in the partition properties of particular fluorescent probes into the coexisting lipid domains [7,8]. However, this last strategy represents only a part of the experimental approach reported in the original paper using fluorescence correlation spectroscopy (FCS) [5]. In our opinion, this strategy constitutes a risky experimental choice as it has been documented repeatedly that the partition properties of fluores-

* Corresponding authors. L.A. Bagatolli is to be contacted at Membrane Biophysics and Biophotonics group/MEMPHYS, Center for Biomembrane Physics, Department of Biochemistry and Molecular Biology, University of Southern Denmark, Campusvej 55, DK-5230 Odense M, Denmark. S. Härtel, Laboratory for Scientific Image processing (SCIAN-Lab), Anatomy and Developmental Biology Program, Faculty of Medicine, University of Chile, Santiago, Chile and Nucleus of Neural Morphogenesis (NEMO), Santiago, Chile.
E-mail addresses: shartel@med.uchile.cl (S. Härtel), bagatolli@memphys.sdu.dk (L.A. Bagatolli).
[1] These authors contribute equally to this article.

0005-2736/$ – see front matter © 2009 Elsevier B.V. All rights reserved.
doi:10.1016/j.bbamem.2009.08.006

cent probes into lipid domains *do not depend on the local phase state* but instead on the chemical environment of the observed lipid domain [2,3,9,10]. This last observation highlights the importance of performing a careful correlation between the probe's partition and the lipid domain's physical properties (structural or dynamical) for individual lipid mixtures in order to ensure proper interpretation of the experimental results (see, for example, references [9,11–13]).

The data obtained from GUVs experiments have been recently used to construct phase diagrams for different lipid mixtures [8,14,15]. Most of these experiments used fluorescent images of GUVs obtained under epifluorescence illumination [15], and in one case, used the probe's diffusion information [14]. In general, the data utilized for the construction of the corresponding phase diagram are the lipid composition where the appearance, persistence, or vanishing of micrometer-sized lipid domains is observed in GUVs at selected temperatures. However, the lateral resolution limit of fluorescence microscopes precludes ascertaining the presence of nanoscopic lipid domains in the utilized lipid mixtures. In this respect, questions have been raised about the accuracy of describing the complete phase diagram of different lipid mixtures using GUVs/fluorescence microscopy. Indeed, some discrepancies have been observed for the palmitoyl-sphingomyelin/POPC/cholesterol ternary mixture's phase diagram obtained from fluorescence microscopy experiments (GUVs labeled with Texas Red-DPPE) [16] and from fluorescence spectroscopy experiments (e.g., FRET in large unilamellar vesicles – LUVs – using NBD-DPPE and Rhodamine-DOPE) [17].

Other criticisms have recently questioned the accuracy of fluorescence microscopy experiments involving GUVs to provide valid information about the lateral structure of membranes. Some laboratories have reported that photooxidation of fluorophores under the microscope (under high illumination power) would affect the membrane lateral scenario [18]. This effect would generate artifacts particularly in those cases where unsaturated lipids are present in the studied mixtures (DOPC and POPC were studied) [19]. In addition, it was claimed that during formation of GUVs, poor equilibration may occur among the lipid mixtures components. This last phenomenon may generate compositional heterogeneity in the final GUV population [19]; that is, a population of GUVs in which the individual vesicles has a different lipid composition. Furthermore, it has been reported that the presence of fluorescent probes strongly affects the lipid miscibility transitions [20]. Taken together, all the above observations pose a significant challenge to the reliability of fluorescence microscopy related work that is being carried out by an increasing number of research groups using GUVs as model systems.

In this context, it is necessary to remark that the current body of reported GUV/fluorescence microscopy experiments (including those used to determine phase diagrams) are solely based on the acquisition of fluorescence images and the measurement of fluorescence probe-related parameters (e.g., partition of probes between the coexisting lipid domains, probe diffusion, and probe's lifetimes and emission shift) at different lipid compositions and temperatures (1–13). The existing data undoubtedly indicate different physical properties between the coexisting lipid domains; however, they do not provide any direct evidence about the correspondence between the lipid domain coexistence observed in GUVs and the coexistence of equilibrium thermodynamic phases. Lyotropic mesophases in phospholipids containing membranes can show in certain situations meta-stability [21]. The timescale for meta-stabilities can range from seconds to months or longer. It is thus of paramount importance in any studies of model membrane systems to validate if equilibrium conditions are present in the system under studied. Failure to do this may lead to entirely fallacious interpretations of the data [21]. Particularly concerning GUVs as model systems, additional quantitative information directly measured from 3D fluorescent images may aid in solving this problem. In other words, the possibility to directly visualize single GUVs allow to obtain quantitative morpho-topological parameters at the level of a single vesicle (such as domain area, perimeter) and use this information to validate thermodynamic principles which set further reaching interpretations on a solid basis.

Major regimes of thermodynamic parameters (temperature and composition), where the system displays phase coexistence between macroscopic domains (with distinct phase characteristics), are a common feature for multicomponent thermodynamic systems at equilibrium. In GUVs, for example, the observed membrane domains may represent such thermodynamic phases. A clear signature of thermodynamic equilibrium at the phase coexistence regime is the achievement of the lever rule, which is a direct consequence of thermodynamic equilibrium principles. The lever rule establishes a simple relationship between extensive properties (number of molecules, area, volume) of the system and particular phase characteristics. By measuring for example the coexisting domain area fractions in GUVs, we can test if these distinct regions satisfy the lever rule. Attainment of this rule will allow invoking a connection between the presence of lipid domains and the presence of equilibrium thermodynamic phases. This type of validation constitutes a “proof of principle experiment” and, to our knowledge, has not been performed in GUVs before. Moreover, a method for systematic quantization of individual 3D images of GUVs has not been described so far.

In this work, we developed and applied image analysis techniques to determine the GUV surface area and the corresponding area fractions of coexisting ordered and disordered lipid domains in different DLPC/DPPC GUV populations of defined composition. We show that the lipid domain area fractions can be used to scrutinize the lever rule, allowing testing whether or not the lipid domain coexistence scenario corresponds with the coexistence of equilibrium thermodynamic phases. This quantitative approach offers a new powerful tool that, in our opinion, will largely improve the quality of the data obtained in GUVs/fluorescence microscopy experiments, opening new possibilities to recover morpho-topological information at the level of single vesicles.

2. Materials and methods

1,2-Lauroyl-*sn*-glycero-3-phosphocholine (DLPC) and 1,2-palmitoyl-*sn*-glycero-3-phosphocholine (DPPC) were purchased at Avanti Polar Lipids (Alabaster, AL, USA). The probes 1,1′-dioctadecyl-3,3,3′,3′-tetramethylindocarbocyanine perchlorate ($DiIC_{18}$) and 2-(4,4-difluoro-5,7-dimethyl-4-bora-3a,4a-diaza-sindacene-3-pentanoyl)-1-hexadecanoyl-sn-glycero-3-phosphocholine (Bodipy-PC) were purchased from Invitrogen (Copenhagen, Denmark).

2.1. Preparation of GUVs and confocal laser scanning fluorescence microscopy experiments

GUVs were prepared following the electroformation method described by Angelova et al. [22] using a custom-built chamber that contains indium-tin-oxide coverslips (ITO, Thin Film Devices, Anaheim, CA, USA) as electrodes as described in Fidorra et al. [23]. This chamber allows preparation and visualization of the GUVs directly in the microscope without removing the vesicles that are attached to the electrode. Briefly, an aliquot of the desired lipid mixture containing the fluorescent probes (<0.3 mol% respect to total lipids) dissolved in organic solvent (Cl_3CH/MetOH 2:1 v/v) was deposited on the center of the conducting surface of the ITO electrode (10 μl of 3 mg/ml lipid stock solution) and smeared with a clean coverslip until the solvent was evaporated. After the removal of the organic solvent, the ITO containing the lipids was assembled into the home-built electroformation chamber [23] and hydrated using MilliQ water (conductance 17.5 MΩ, Millipore, Billerica, MA, USA) for about

30 min at a temperature above the liquidus line of the mixture phase diagram (55 °C for all the samples). The hydration step was followed by the application of an AC field using a function generator (Vann Draper Digimess Fg 100, Stenson Derby UK) with an amplitude of 1.3 V and a frequency of 10 Hz. The electroformation was carried out for 15 min. Subsequently, the GUVs chamber was cooled to 20 °C in a time span of approximately 5 h in an oven (J.P. Selecta, Barcelona, Spain) using a temperature ramp (~0.2 °C/min). The last step was done in order to achieve equilibrium conditions in our samples. Once the solution reached room temperature, the vesicles were directly observed in the microscope. The temperature during image acquisition was controlled to be 20.0 ± 0.5 °C.

Confocal Image stacks were acquired on both a Zeiss Axiovert 200, Pascal-5 and in a Zeiss LSM 510 Meta confocal laser scanning fluorescence microscopes. A C-Apochromat 40× water immersion objective with a NA 1.2 was used in our experiments. Two channel image stacks were acquired using multi-track mode. Argon and NeHe lasers (488 and 543 nm) were used as excitation sources. Both laser lines were reflected to the sample through the objective using a dichroic mirror (HFST 488/543/633). The fluorescence emission collected through the objective was directed to the PMT detectors using a mirror. Beam splitters were used to eliminate remnant scatter from the laser sources (NFT 490 and NFT 545 for the 488 and 543 nm excitation sources, respectively). Additional filters were incorporated in front of the PMT detectors in the two different channels to measure the fluorescent intensity, i.e., a long pass filter >560 nm for DiIC18 and a band pass filter 515 ± 15 nm for Bodipy-PC. The acquired intensity images were checked to avoid PMT saturation and loss of offsets ($0 \leq I \leq 255$) by carefully adjusting the laser power, the detector gain, and the detector offset. The image stacks were acquired at a sampling rate of 70 nm for Δx and Δy, and 340 nm for Δz, which is slightly above the Nyquist frequency (see Fig. 1), which was calculated to ~40 nm for Δx and Δy, and ~140 nm for Δz with Huygens Scripting Software (Scientific Volume Imaging, Hilversum, Netherlands). The sampling above the Nyquist frequency was necessary to guarantee sufficient scan speed, which minimizes vesicle movement and photobleaching, especially in the Bodipy-PC channel. The obtained confocal raw fluorescence image stacks were deconvolved by Huygens Scripting Software using an algorithm based on the Classic Maximum Likelihood Estimator (see Fig. 2, left column). All image-processing routines described below were developed in one of the author's laboratories (www.scian.cl) on the basis of IDL 7.0 (Interactive Data Language, ITT, CO, USA), including interactive tools for the segmentation of different regions of interest (ROIs), for visualization, 3D reconstruction, and determination of lipid surface areas.

2.2. Segmentation, 3D reconstruction, and determination of lipid surface areas in GUVs

Segmentation of the ordered and disordered lipid domains areas was performed successively in the *xy* planes, prior to the reconstruction of the GUVs in the third dimension (Fig. 2). For this purpose, we applied a series of image filters that have been developed for the segmentation of coexisting lipid phases in lipid monolayers [24,25]. For each image of the two channel stack, we applied (i) subtraction of the respective opposite channel intensity, (ii) threshold setting in the intensity histogram of the subtracted images which creates binary image masks, and (iii) application of morphological filling or removal of remaining holes or patches (Fig. 2). Finally, we applied an active contour model, which parameterizes internal forces like contour elasticity (α) or rigidity (β) [26]. Elasticity and rigidity mimic physical contour properties like elastic (stretching) energy or bending energy. In addition, we derived external force fields from intensity gradients after the application of Laplace filters to the original image data by an iterative algorithm,

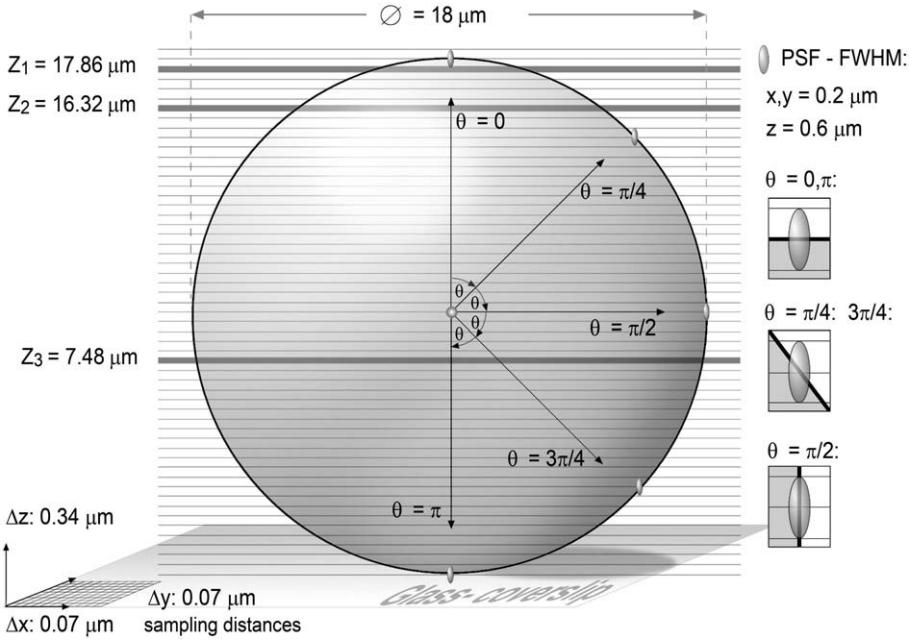

Fig. 1. Representative scheme of the acquisition parameters, dimensions, and geometry between GUVs and PSF inherent to confocal laser scanning microscopy. The 2D scheme uses sphere coordinates: $r = 9$ μm, $0 \leq \theta \leq \pi$, and $0 \leq \varphi \leq 2\pi$, with a rotational symmetry for φ. The dimension of the PSF is characterized by FWHM values: ~0.2 μm for *xy* plane and ~0.6 μm for the *z*-axis. The *xyz*-sampling distances were set to 0.07 μm for the *xy* plane and 0.34 μm for the *z*-axis. The θ-dependent geometry between the GUV surface and the PSF leads to different acquisition scenarios: (i) at $\theta = 0$ or π, the GUV surface is oriented parallel to the *xy* plane of the PSF, which provides the best possible resolution for the lipid domain morphology onto the *xy* planes of the confocal images (see enhanced *xy* slice at $z_1 = 17.86$ μm and Fig. 2A), (ii) at $\theta = \pi/4$ or $3\pi/4$, the GUV surface is oriented diagonally to the *xy* plane of the PSF, which leads to the acquisition of relatively 'thick' membrane slices in the *xy* planes of the confocal images (see slice at $z_2 = 16.32$ μm and Fig. 2A), and (iii) at $\theta = \pi/2$, the GUV surface is oriented vertically to the *xy* plane of the PSF which leads to relatively 'thin' membrane slices in the *xy* plane of the confocal images, but fluorescence signals are integrated along the GUV-surface collinear to the elongated *z*-axis of the PSF (see slice at $z_3 = 7.48$ μm and Fig. 2A).

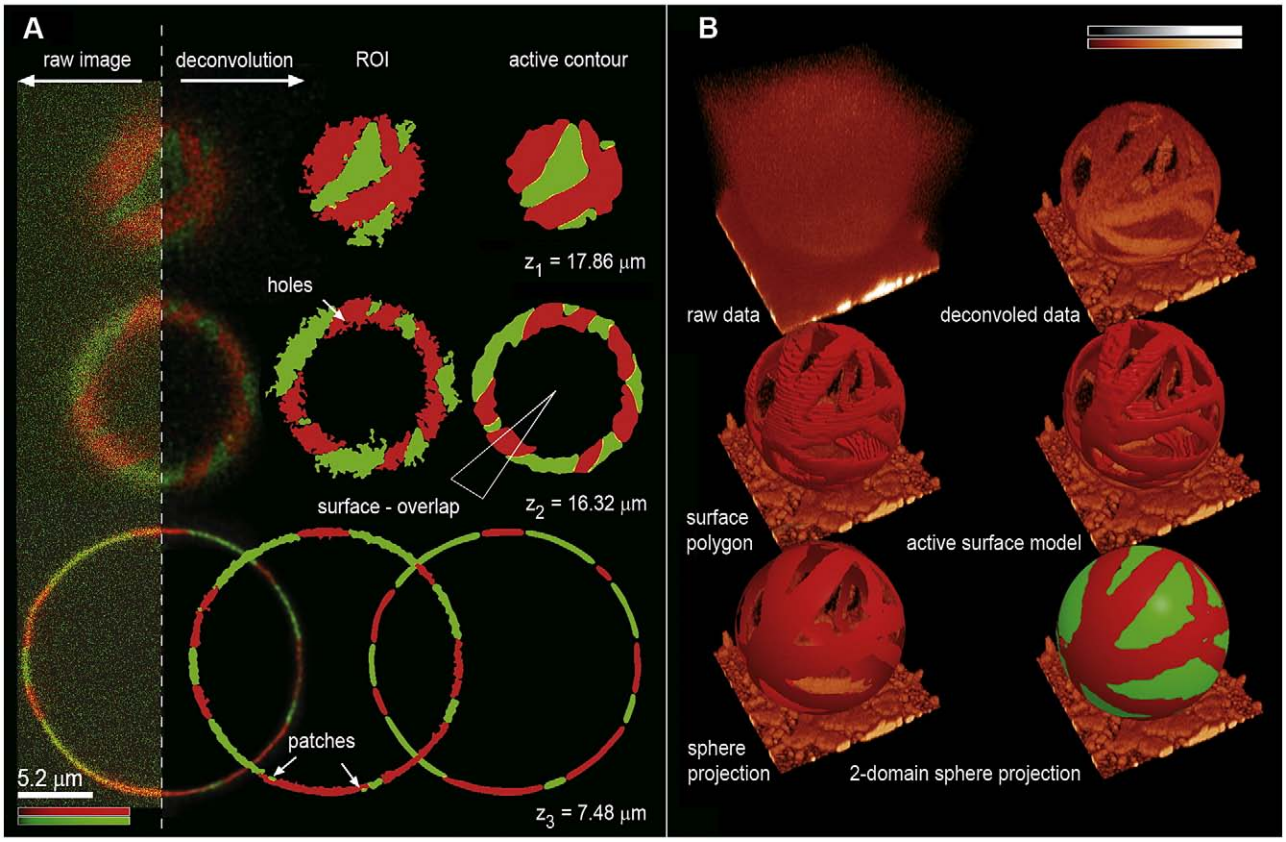

Fig. 2. Sequential image analysis leads to the segmentation of the disordered and ordered lipid domains areas of GUVs (DLPC/DPPC = 30/70 mol%) in 2D slices (A) and to the reconstruction of surface areas in 3D stacks (B). (A) Left column shows three representative 2D slices at $z_1 = 17.86$ µm, $z_2 = 16.32$ µm, and $z_3 = 7.48$ µm (see GUV acquisition scheme in Fig. 1). Left half shows raw image data and right half shows deconvolved data with improved signal to noise ratio. Center column presents ROIs for the disordered (green) and ordered (red) lipid domains. ROIs were obtained by thresholds in the intensity histograms and binary filling/removal of 0.125 µm^2 holes/patches. Right column presents ROIs after the application of active contour models and final removal of remaining 0.125 µm^2 patches. Scale bar presents 5.2 µm. Red and green LUTs for 8-bit images are constant for raw and deconvolved images. (B) Segmentation of ordered lipid domain areas of GUVs from 3D image stacks. First row presents raw data before and after deconvolution with identical LUTs and opacity tables (upper right corner). Second row left shows 3D surface polygons after superposition of 2D-active contour ROIs (right column in panel A), and a 3D-active surface model (right) that smoothes lipid domain boundaries and z-stairs. The bottom row shows the projection of the outer and the inner side of the 3D-active surface meshes onto a fitted sphere, which removes all remaining z-steps and allows the direct calculation of the lipid domain surfaces from the polygon areas (see Materials and methods section). The segmented disordered lipid domains (green) are projected below the ordered lipid domains (red).

known as Generalized Gradient Vector Flows (GGVF) [27]. The GGVF pulls contour points towards the object borders. The balance between internal and external forces is solved by the Euler-Lagrange condition for the minimization of the energy functional E for the parametric curve $C(s) = [x(s), y(s)] = \{xi, yi\}$, $s \in [0, 1]$:

$$E = \int_0^1 0.5 \cdot \left[\alpha|\underline{C}'(s)|^2 + \beta|\underline{C}''(s)|^2\right] + E_{\text{ext}}(\underline{C}(s))\mathrm{d}s \qquad (1)$$

C′ and C″ refers to first- and second-order derivatives in respect to s. Precise assimilation of the contours towards the morphology of lipid domains was achieved by setting the appropriate model parameters. Besides α and β, the model contains parameters for the ambient viscosity (γ) that modulates the step size for each iteration, an external force coefficient (k) that controls the strength of the external force field, and the number of iterations (t). The quality of the segmented ROIs was controlled interactively by overlaying the original fluorescent images with the masks of each channel.

For 3D reconstruction of the surface domains, 2D active contour ROIs were connected by a simple overlap criterion and a first 3D presentation of the domain morphology was obtained by surface polygons (Fig. 2B). Surface polygons were calculated by a method similar to the marching cubes algorithm [28], using the 'shade-volume' algorithm included in the IDL library. The definition of domain contours in 3D was improved significantly by the application of a 3D-active surface model, a direct expansion of the active contour model with the parametric surface $C(s) = [x(s), y(s), z(s)] = \{xi, yi, zi\}$, $s \in [0, 1]$ and a 3D GGVF [29]. As before, precise assimilation of the active surface towards the morphology of the domain structures was controlled interactively by setting the appropriate parameter combination α, β, γ, k, and t.

2.3. Determination of lipid domain areas in GUVs

The determination of lipid domain areas was performed after the projection of the active surfaces onto perfect spheres that were approximated to the segmented ROIs (see sphere projection in Fig. 2B). Projection of the active surface model onto perfect spheres was necessary for different reasons. First, because of the extension of the point spread function (PSF) of laser scanning microscopes, the fluorescent signal of the thin lipid bilayer (4–6 nm) is convolved into a Gauss-like intensity distribution with FWHM (full with at half maximum) values of ~250 nm in the xy plane and ~600 nm in the z-axis (calculated with Huygens Scripting Software). Therefore, confocal representations of structures beyond the resolution limit lead to the segmentation of relatively thick 2D ROIs and, in consequence, thick embedding surfaces (see surface polygons in Fig. 2B). The 'outer' surface area overestimates the 'real' surface area of a GUV, while the 'inner' surface underestimates it. In addition,

lipid domains on GUVs can form heterogeneous surface pattern. If domains become small, the embedding surfaces include an increasing degree of surface area with normal vectors perpendicular to the surface of a GUV. This leads to a size and morphology dependent overestimation of the 'real' surface area of lipid domains on the GUV. Second, the active surface model cannot eliminate all z-stairs without compromising the domain morphology in the *xy* plane (see Fig. 2B, active surface model). These stairs lead to artificially enhanced surface areas.

To eliminate this artifact, we projected all nodes of the surface mesh to 'perfect spheres' which were derived from the experimental data in the following way: (i) we calculated 200 spheres from randomly selected data quadruples of the active surface models, (ii) we ordered these spheres by size, and (iii) calculated mean values for the centre position (x, y, z) and the radius (r) from 40 spheres around the median of the size distribution. The quality of the calculated 'perfect spheres' was controlled visually by direct comparison with the experimental data. Finally, the nodes of the active surface models were projected onto the perfect sphere surface (Fig. 2B), and lipid domain areas were calculated by summing all polygon areas and final division by 2.

2.4. Lever rule and area analysis

One of the observable quantities for the two classes of lipid domains is their respective areas A^{so} (solid ordered, gel) and A^{ld} (liquid disordered), form the total area A of the GUV:

$$A = A^{so} + A^{ld} \tag{2}$$

However, it is important to note that the ability to distinguish two characteristic environments on a vesicle (for example, different physical properties) is not sufficient to denote them as equilibrium thermodynamic phases. To establish this, it is required that they are characterized by well-defined "densities" (ratios between thermodynamic extensive variables), like the molecular area $a^{\alpha}=A^{\alpha}/N^{\alpha}$ and composition expressed by the molar fraction $x^{\alpha}=N_1^{\alpha}/N^{\alpha}$. N^{α} and N_1^{α} is the total number of molecules and number of components "1" in domain type $\alpha=$ ld. Consistency with thermodynamic equilibrium requires that the Lever rule is fulfilled:

$$\frac{N^{ld}}{N} = \frac{x^{so} - x}{x^{so} - x^{ld}} \tag{3}$$

where $x=N_1/N$ is the overall molar fraction of DLPC. Here N is the total number of molecules in the vesicle. These relations can also be expressed as area ratios, e.g:

$$\left[\frac{A^{ld}}{A^{so}}\right](x) = \frac{a^{ld}}{a^{so}}\frac{x^{so} - x}{x - x^{ld}} \tag{4}$$

Our test of whether the conditions for equilibrium thermodynamic two-phase coexistence is fulfilled is obtained by a χ^2 analysis according to [30]. In other words, from measurements of A^{ld} / A^{so} (for various mole fractions x in the coexistence region observed in the lipid mixture's phase diagram) it should be possible to recover the appropriate phase boundaries at a given temperature (i.e. x^{so} and x^{ld}) only if the lipid domains correspond to equilibrium thermodynamic phases. In our analysis the molecular cross-sectional areas for the coexisting phases are assumed to be those previously reported for DPPC in the solid ordered phase a^{so}~46 Å^2 [31], and DLPC in the liquid disordered phase a^{ld} ~65 Å^2 [32]. Indeed, it was reported that in these type of binary mixtures, lipid mixing causes minor changes in the lipid's cross-sectional areas within the individual phases [33].

3. Results

3.1. Determination of lipid domain areas in GUVs

For each lipid composition, we acquired and analyzed 11-14 vesicles with interactive image processing approaches that are outlined in Figs. 1 and 2. One of the most critical parts for this analysis is to precisely define the boundaries between the two coexisting membrane regions. As we show in Fig. 2A, left column, deconvolution significantly improves the signal to noise ratio which presents an essential step for the reliable analysis of fluorescence pattern of microscopic structures near the resolution limit [34]. The quality of the segmentation of the lipid phases was checked visually by consecutive superposition of the deconvolved images with the corresponding ROIs. We crosschecked the results of the lipid domain segmentation and final area determination performed by different investigators for identical GUVs and found variations below 3% among the individual examinations. Fig. 3A, B shows the distribution of the disordered lipid domain surface area (A^{ld}), the ordered lipid domain surface area (A^{so}), and the overlapping lipid domain's surface areas for a single GUV population (DLPC/DPPC = 60/40 mol%). For the presented composition, the mean area fractions $A^{so}/(A^{ld}+A^{so})$ and $A^{ld}/(A^{ld}+A^{so})$ yielded 0.27 and 0.73 which were calculated from 13 vesicles with a standard deviation (SD) of 0.073 and standard error (SE) of 0.02. SD and SE values were very similar for all experimental mixtures: for 50, 40, 30, and 20 mol% DLPC, SD/SE yielded 0.066/0.016, 0.044/0.013, 0.044/0.013, and 0.056/0.015. As Fig. 3B shows, the sum of both phase areas $A^{so}+A^{ld}$ is about 10% higher than the surface area of the perfect spheres: for a total of 62 GUVs analyzed, the mean value of $(A^{so}+A^{ld})$ / (perfect sphere surface area) yields 1.1 (SD/SE = 0.11/0.015). We propose that different effects may contribute to explain this phenomenon:

1) A spatial overlap of the signal coming from the two probes. This phenomenon is observed at the lipid domain boundaries and may be explained considering:
   (a) Different partition properties of the probes in this particular region. We expect that the properties of this region are not equal to those observed in the bulk phases.
   (b) The existence of nanoscopic domains, either non-resolvable or at the limit of microscopic resolution, exerting a different distribution of the probes at the domain boundaries may explain this observation.
2) The geometric properties between the microscopic PSF and the orientation of the GUV surface as outlined in Fig. 1 and shown in Fig. 2A. Using sphere coordinates $r \geq 0$ µm, $0 \leq \theta \leq \pi$, $0 \leq \varphi \leq 2\pi$, the following situations must be considered:
   (a) $\theta \approx 0$ or π guarantee the best projections of the GUV domain morphologies onto the xy planes of the images (FWHM-values of PSF ≈ 0.2 µm).
   (b) $\theta \approx \pi/4$ or $3\cdot\pi/4$ lead to increased domain overlap along r, since the GUV surface is orientated diagonally in respect to the *xy* plane (Fig. 1 and Fig. 2A $z_2 = 16.32$ µm).
   (c) for $\theta \approx \pi/2$, the GUV surfaces pass perpendicularly through the *xy* plane of the PSF (FWHM-values ≈ 0.6 µm) which leads to a decreased resolution due to an increased integration of fluorescence signals along the *z*-axis. However, the result of the applied segmentation procedure does not lead to significant overlap in this region (Fig. 2A, $z_3 = 7.48$ µm).

The second argument is probably more relevant considering the technical aspect of our experiments (although we are not completely disregarding the alternative explanations exposed in item 1). However, in light of the results presented in the next section, it is clear that this phenomenon is not affecting the quality of the obtained results significantly.

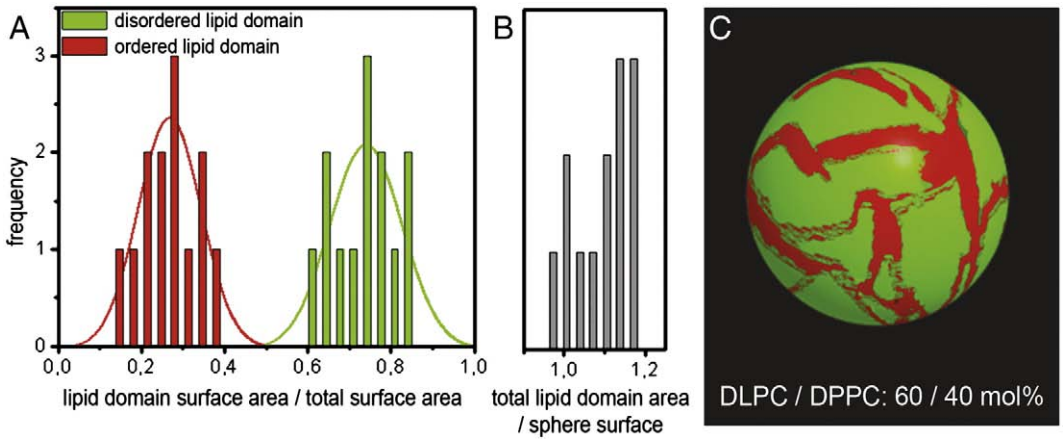

Fig. 3. Distribution of the disordered, the ordered, and the overlapping lipid domain surface areas for a single GUV population (DLPC/DPPC = 60/40 mol%). (A) Histogram of A^{ld} (green) and A^{so} (red) normalized by total surface area ($A^{so}+A^{ld}$) is plotted together with a fitted Gauss distribution for the respective data. (B) Histogram of the total lipid domain area ($A^{so}+A^{ld}$) divided by the perfect sphere surfaces. The mean value is 1.09 (SD/SE = 0.068/0.019). (C) Surface reconstruction of a representative GUV composed of DLPC/DPPC = 60/40 mol%. Surface for disordered (green), ordered (red), and overlapping lipid domain areas. The perfect sphere diameter of the presented GUV is 11.4 μm.

3.2. Lever rule and area analysis

Figure 4 plots the obtained area ratios at different molar fractions of DPPC for the disordered and ordered lipid domains (A^{ld}/A^{so}), which were used to perform the χ^2 analysis of the lever rule formulation presented in Eq. 4. The χ^2 analysis was performed using the observed lipid domains obtained from the raw data of the entire GUV population (open round symbols in Fig. 4). Representative GUVs images at different DPPC molar fractions (X_{DPPC}) are also included in Fig. 4. The χ^2 fit gives the following results for the two phase boundaries: $x^{ld} = 0.18 \pm 0.04$, $x^{so} = 0.84 \pm 0.04$, results that are very well in line with those that are predicted from the DLPC/DPPC mixture phase diagram at 20 °C (see Fig. 5).

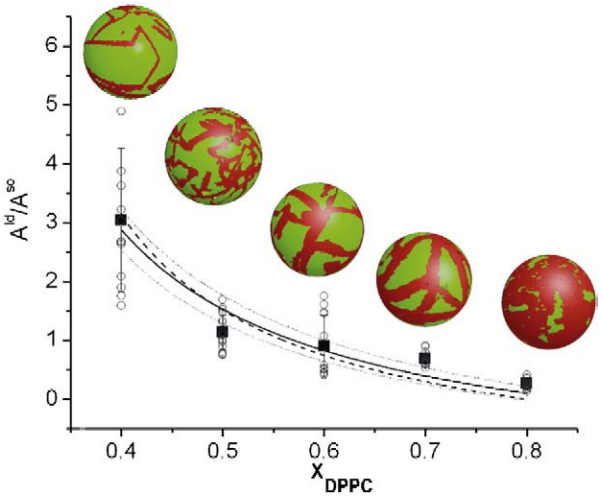

Fig. 4. Area ratios A^{ld}/A^{so} versus the lipid fraction X_{DPPC} for five different GUV populations: $X_{DPPC} = 0.4$, 0.5, 0.6, 0.7, and 0.8. The experimental data of A^{ld}/A^{so} is plotted for 62 GUVs (○) in combination with the respective mean values (■) and the corresponding SD. The solid line represents the result of a χ^2 fit for $\left[\frac{A^{ld}}{A^{so}}\right](x) = \frac{a^{ld}}{a^{so}} \frac{x^{so}-x}{x-x^{ld}}$ that yields $x^{ld} = 0.18 \pm 0.04$ and $x^{so} = 0.84 \pm 0.04$. The dotted lines correspond to the 95% confidence bands of the fitted curve. The dashed curve was calculated using $x^{ld} = 0.22$ and $x^{so} = 0.80$, which were estimated from previously published experimental data ($x^{ld} = 0.22$, $x^{so} = 0.79$, (41)) and theoretical data ($x^{ld} = 0.22$, $x^{so} = 0.81$, see Fig. 5). Surface projections for 5 representative GUVs are plotted for each corresponding lipid fraction.

4. Discussion

In spite of the high number of publications using the giant vesicles/fluorescence microscopy approach to study membrane lateral heterogeneity, there is a lack of a strict validation of the equilibrium thermodynamic nature of the coexisting lipid domains observed in GUVs. As shown for the first time in this work, lipid domain area fractions can be retrieved from GUVs using image analysis methods and this information can be used to interrogate the system with predictions extracted from equilibrium thermodynamic phase diagrams (e.g., the lever rule, Fig. 4).

4.1. Image analysis

The reliable access of lipid domain morphology and topology in 3D bilayers presents an important step towards a quantitative analysis of membrane-related features in this widely used model system. By exploring the previously reported work on GUVs/fluorescence microscopy, few papers mention measurements of area fractions of coexisting lipid domains in GUVs [8,15,34,35]. However, we did not find accurate descriptions of the utilized method (e.g., if the

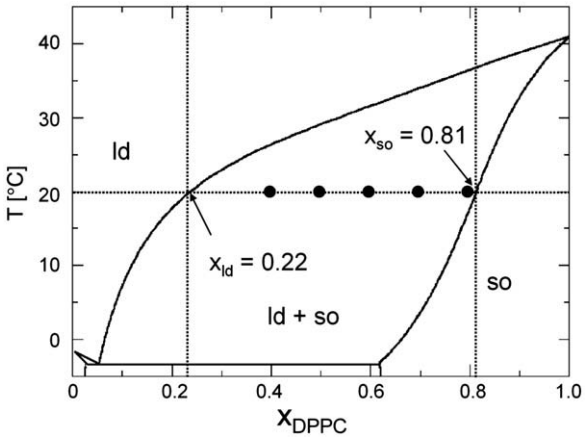

Fig. 5. Theoretical phase diagram for DLPC/DPPC calculated according to [33]. The black dots along the tie line represent the DLPC/DPPC mixture's molar fractions used in this work. The phase boundaries (x^{ld} and x^{so}) obtained at 20 °C from this phase diagram are also indicated in the figure (black arrows).

calculations are performed in single images or 3D pictures of the GUVs) nor any statistical information on the explored GUV population. Therefore, we consider highly relevant to develop and introduce image analysis approaches that allows quantitative information from single GUVs.

During recent years, the precise quantification of 2D domain morpho-topologies in different lipid monolayer systems has opened the access towards the understanding of self-organizing and enzyme-driven pattern formation far beyond the capacities of visual perception [24,25,26]. The quantitative access to geometrical features of lipid domain pattern from microscopic image series requires flexible mathematical routines with the capability to handle a series of limits that are intrinsic to the respective experimental imaging setup. For the reliable segmentation of 2D lipid domains, active contour models have been implemented to counteract experimental drawbacks arising from digital oversampling/undersampling or poor signal/noise ratios [27]. In 3D confocal microscopy, undersampling of the GUV data in respect to the Nyquist Sampling Theorem is necessary during data acquisition to minimize sample fluctuations and potential photobleaching effect on the fluorescent probe during the data acquisition. As we show in Figs. 1 and 2, the asymmetry of the PSF in the *z*-axis leads to additional geometric problems for the reliable reconstruction of surface domain morphologies which requires careful future consideration. Nevertheless, the active surface model prior to the sphere projection leads to a reasonable first approximation of domain morphologies (Fig. 2). It must be acknowledged that the effort to improve image processing routines for the quantification of GUV domain morpho-topologies is only applicable if basic thermodynamic features can be confirmed reliably in the GUV preparations.

Our approach to access domain surface areas leads to relative small variations inside particular GUV populations (see Fig. 3). We consider fluctuations of the SD from 4.4% to 7.3% and SE from 1.3% to 2.0% an excellent result. We had expected much higher values, since vesicle preparation, microscopic acquisition, and interactive image analysis present accumulating error sources. If quantitative data for surface areas have to be extracted from an unknown vesicle population, SE values are appropriate, since the interest is focused on the uncertainty for the mean value of the determined surface area. In our opinion, standard errors between 1.3% and 2.0% in respect to the total vesicle surface are acceptable for many experimental strategies.

4.2. Lipid domains and equilibrium thermodynamic phases

The different membrane regions observed in DLPC/DPPC mixtures have previously been correlated with liquid disordered (ld) and solid ordered (so) phases based in experiments done with the LAURDAN probe [2,3] and FCS experiments performed with similar fluorescent probes to those used here [5]. However, such correlation, i.e., liquid disordered or solid ordered, was done due to their apparent relationship with the well-established solid-ordered/liquid-disordered phase coexistence obtained, e.g., by differential scanning calorimetry experiments [36]. In fact the observation of different regions in GUVs experiments (including the determination of their local physical parameters [2,3,5]) does not provide all the information required to fully corroborate if the coexisting domains fulfill the characteristics of equilibrium thermodynamics phases. Such a relationship is not obvious since the thermodynamic and structural characterization (e.g., X-ray, NMR and DSC) of lipid membranes requires large quantities, like multilamellar vesicles or oriented supported multilayers (MLVs), where even weak couplings between membranes may stabilize distinct thermodynamic phases. Such three-dimensional couplings are absent for GUVs. Instead, GUV's membranes are subject to out of plane conformational fluctuations, which may hamper the formation of macroscopic phases due to budding phenomena [37], curvature frustration [38,39], or critical fluctuations. In addition, the presence of long-lived percolating solid ordered-like structures in the coexistence region [40] may distort any interpretation.

The phase boundaries x^{so} and x^{ld} calculated by the presented χ^2 analysis are consistent with those obtained using a theoretical thermodynamic description of DLPC/DPPC mixture according to [33] (Fig. 5) and previously reported experimental data [41]. The evidence is shown in Fig. 4 where an additional curve (dashed line), calculated using Eq. 4 with the aforementioned phase boundaries, is included for comparison. Taken as a whole, the obtained results indicate that the domains observed in the GUVs can be considered equilibrium thermodynamic phases. Our results also challenge the existence of high compositional heterogeneity claimed to exist among GUVs obtained from the same preparation [19]. We reasoned that if such high compositional heterogeneity exists, it would be very unlikely to fit the lever rule using data obtained randomly from 11 to 14 vesicles. This leads to another important point, i.e., that the composition of a relative small group of single vesicles may be representative of the whole GUV population. This last fact is in agreement with previous work reporting a good correlation between the thermotropic behavior observed in GUVs and solution of liposomes (MLVs; using DSC, FTIR, and NMR using solutions [3,6,23,42]).

5. Conclusions

The presented approach provides novel quantitative information from GUVs/fluorescence microscopy experiments. This allows us to perform a proof of principle experiment and demonstrate for first time that lipid domains in DLPC/DPPC GUVs correspond with equilibrium thermodynamic phases. Our observations challenge the presence of artifacts caused by inherent aspects of the utilized experimental method (e.g., effects of the fluorescent probes, or the GUV preparation protocol) previously mentioned in the literature. We are confident that the presented approach can be extended to corroborate whether or not the observed lipid domain coexistence in GUVs composed of ternary mixture containing cholesterol corresponds to equilibrium thermodynamic phases. This may well reconcile the aforementioned discrepancies reported between phase diagrams of palmitoyl-sphingomyelin/POPC/cholesterol using GUVs [16,43] or LUVs [17]. In addition, we are currently exploring new analysis based on quantification of domain area fractions in GUVs, with the specific aim to track orientation of tie lines at the phase coexisting regions of ternary mixtures phase diagrams [44]. Last but not least, we envisage that the proposed image analysis will increase the potentialities in quantifying additional 3D morpho-topological lipid domain features. We believe that the presented method will help to extract new quantitative parameters from the lipid domains in 3D (perimeter, curvature, etc.) in order to improve our understanding of lateral separation in membranes in the future.

Acknowledgments

The authors thank N. Contreras from Area Kreativa for support with the figures and Dr. J. Cowan for his help revising English style and grammar. Research in the laboratory of L.A.B. is funded by grants from Forskningsrådet for Natur og Univers (FNU, Denmark), Forskningsrådet for Sundhed og Sygdom (FSS), and the Danish National Research Foundation (which supports MEMPHYS-Center for Biomembrane Physics). Research in SCIAN-Lab (S.H.) is funded by FONDECYT (1060890 and 1090246) and FONDEF (D07I1019) both CONICYT (Chile), and the Millennium Scientific Initiative (ICM P04-068-F). The interdisciplinary collaboration between L.A.B.'s and S.H.'s laboratories was supported by FONDECYT (7060265 and 7080031), CONICYT Chile and MEMPHYS, Center for Biomembrane Physics, University of Southern Denmark, Odense, Denmark.

References

[1] L.A. Bagatolli, E. Gratton, Two-photon fluorescence microscopy observation of shape changes at the phase transition in phospholipid giant unilamellar vesicles, Biophys. J. 77 (4) (1999) 2090–2101.
[2] L.A. Bagatolli, E. Gratton, A correlation between lipid domain shape and binary phospholipid mixture composition in free standing bilayers: a two-photon fluorescence microscopy study, Biophys. J. 79 (1) (2000) 434–447.
[3] L.A. Bagatolli, E. Gratton, Two photon fluorescence microscopy of coexisting lipid domains in giant unilamellar vesicles of binary phospholipid mixtures, Biophys. J. 78 (1) (2000) 290–305.
[4] C. Dietrich, L.A. Bagatolli, Z.N. Volovyk, N.L. Thompson, M. Levi, K. Jacobson, E. Gratton, Lipid rafts reconstituted in model membranes, Biophys. J. 80 (3) (2001) 1417–1428.
[5] J. Korlach, P. Schwille, W.W. Webb, G.W. Feigenson, Characterization of lipid bilayer phases by confocal microscopy and fluorescence correlation spectroscopy, Proc. Natl. Acad. Sci. U. S. A. 96 (15) (1999) 8461–8466.
[6] G.W. Feigenson, J.T. Buboltz, Ternary phase diagram of dipalmitoyl-PC/dilauroyl-PC/cholesterol: nanoscopic domain formation driven by cholesterol, Biophys. J. 80 (6) (2001) 2775–2788.
[7] T. Baumgart, G. Hunt, E.R. Farkas, W.W. Webb, G.W. Feigenson, Fluorescence probe partitioning between Lo/Ld phases in lipid membranes, Biochim. Biophys. Acta 1768 (9) (2007) 2182–2194.
[8] S.L. Veatch, S.L. Keller, Seeing spots: complex phase behavior in simple membranes, Biochim. Biophys. Acta 1746 (3) (2005) 172–185.
[9] L.A. Bagatolli, To see or not to see: lateral organization of biological membranes and fluorescence microscopy, Biochim. Biophys. Acta 1758 (10) (2006) 1541–1556.
[10] J.E. Shaw, R.F. Epand, R.M. Epand, Z. Li, R. Bittman, C.M. Yip, Correlated fluorescence-atomic force microscopy of membrane domains: structure of fluorescence probes determines lipid localization, Biophys. J. 90 (6) (2006) 2170–2178.
[11] K. Bacia, P. Schwille, Fluorescence correlation spectroscopy, Methods Mol. Biol. 398 (2007) 73–84.
[12] A. Celli, S. Beretta, E. Gratton, Phase fluctuations on the micron-submicron scale in GUVs composed of a binary lipid mixture, Biophys. J. 94 (1) (2008) 104–116.
[13] R.F. de Almeida, J. Borst, A. Fedorov, M. Prieto, A.J. Visser, Complexity of lipid domains and rafts in giant unilamellar vesicles revealed by combining imaging and microscopic and macroscopic time-resolved fluorescence, Biophys. J. 93 (2) (2007) 539–553.
[14] N. Kahya, D. Scherfeld, K. Bacia, B. Poolman, P. Schwille, Probing lipid mobility of raft-exhibiting model membranes by fluorescence correlation spectroscopy, J. Biol. Chem. 278 (30) (2003) 28109–28115.
[15] S.L. Veatch, S.L. Keller, Separation of liquid phases in giant vesicles of ternary mixtures of phospholipids and cholesterol, Biophys. J. 85 (5) (2003) 3074–3083.
[16] S.L. Veatch, S.L. Keller, Miscibility phase diagrams of giant vesicles containing sphingomyelin, Phys. Rev. Lett. 94 (14) (2005) 148101.
[17] R.F. de Almeida, L.M. Loura, A. Fedorov, M. Prieto, Lipid rafts have different sizes depending on membrane composition: a time-resolved fluorescence resonance energy transfer study, J. Mol. Biol. 346 (4) (2005) 1109–1120.
[18] A.G. Ayuyan, F.S. Cohen, Lipid peroxides promote large rafts: effects of excitation of probes in fluorescence microscopy and electrochemical reactions during vesicle formation, Biophys. J. 91 (6) (2006) 2172–2183.
[19] J. Zhao, J. Wu, H. Shao, F. Kong, N. Jain, G. Hunt, G. Feigenson, Phase studies of model biomembranes: macroscopic coexistence of Lalpha + Lbeta, with light-induced coexistence of Lalpha + Lo Phases, Biochim. Biophys. Acta 1768 (11) (2007) 2777–2786.
[20] S.L. Veatch, S.S. Leung, R.E. Hancock, J.L. Thewalt, Fluorescent probes alter miscibility phase boundaries in ternary vesicles, J. Phys. Chem., B 111 (3) (2007) 502–504.
[21] J. Seddon, G. Cevc, Lipid Polymorphism: structure and stability of lyotropic mesophases of phospholipids, in: G. Cevc (Ed.), Phospholipid Handbook, Marcel Dekker Inc, New York-Basel-Hong Kong, 1993, pp. 403–454.
[22] M.I. Angelova, S. Soléau, MeléardP , J.F. Fauco, P. Bothorel, Preparation of giant vesicles by external AC fields. Kinetics and applications, Prog. Colloid Polym. Sci. 89 (1992) 127–131.
[23] M. Fidorra, L. Duelund, C. Leidy, A.C. Simonsen, L.A. Bagatolli, Absence of fluid-ordered/fluid-disordered phase coexistence in ceramide/POPC mixtures containing cholesterol, Biophys. J. 90 (12) (2006) 4437–4451.
[24] M.L. Fanani, S. Hartel, R.G. Oliveira, B. Maggio, Bidirectional control of sphingomyelinase activity and surface topography in lipid monolayers, Biophys. J. 83 (6) (2002) 3416–3424.
[25] S. Hartel, M.L. Fanani, B. Maggio, Shape transitions and lattice structuring of ceramide-enriched domains generated by sphingomyelinase in lipid monolayers, Biophys. J. 88 (1) (2005) 287–304.
[26] L. De Tullio, B. Maggio, S. Hartel, J. Jara, M.L. Fanani, The initial surface composition and topography modulate sphingomyelinase-driven sphingomyelin to ceramide conversion in lipid monolayers, Cell Biochem. Biophys. 47 (2) (2007) 169–177.
[27] M. Kass, A. Witkin, D. Terzopoulos, Snakes: active contour models, Int. J. Comput. Vis. 1 (1988) 321–331.
[28] W. Lorenson, H.E. Cline, Marching cubes: a high resolution 3D surface construction algorithm, Comput. Graph. 21 (1987) 163–169.
[29] S. Härtel, J. Jara, C.G. Lemus, M.L. Concha, Morpho-topological analysis of asymmetric neuronal morphogenesis in developing zebrafish, in: J.M. Tavares, J. Nata (Eds.), Computational Modelling of Objects Represented in Images. Fundamentals, Methods and Applications, Taylor and Francis Group, 2007, pp. 215–220.
[30] Numerical Recipes, FORTRAN 77, Cambridge University Press 2001.
[31] O. Albrecht, H. Gruler, E. Sackmann, Polymorphism of phospholipid monolayers, J. Phys. (France) 39 (3) (1978) 301–313.
[32] J.F. Nagle, S. Tristram-Nagle, Structure of lipid bilayers, Biochim. Biophys. Acta 1469 (3) (2000) 159–195.
[33] J.H. Ipsen, O.G. Mouritsen, Modelling the phase equilibria in two-component membranes of phospholipids with different acyl-chain lengths, Biochim. Biophys. Acta 944 (2) (1988) 121–134.
[34] C. Fink, F. Morgan, L.M. Loew, Intracellular fluorescent probe concentrations by confocal microscopy, Biophys. J. 75 (4) (1998) 1648–1658.
[35] A. Tian, C. Johnson, W. Wang, T. Baumgart, Line tension at fluid membrane domain boundaries measured by micropipette aspiration, Phys. Rev. Lett. 98 (20) (2007) 208102.
[36] S. Mabrey, J.M. Sturtevant, Investigation of phase transitions of lipids and lipid mixtures by sensitivity differential scanning calorimetry, Proc. Natl. Acad. Sci. U. S. A. 73 (11) (1976) 3862–3866.
[37] R. Lipowsky, Domain-induced budding of fluid membranes, Biophys. J. 64 (1993) 1133–1138.
[38] P.L. Hansen, L. Miao, J.H. Ipsen, Fluid lipid bilayers: intermonolayer coupling and its thermodynamic manifestations, Phys. Rev. E 58 (1998) 2311–2324.
[39] J.L. Harden, F.C. MacKintosh, Shape transformations of domains in mixed-fluid films and bilayer membranes, Europhys. Lett. 28 (7) (1994) 495–500.
[40] C. Leidy, T. Kaasgaard, J.H. Crowe, O.G. Mouritsen, K. Jorgensen, Ripples and the formation of anisotropic lipid domains: imaging two-component supported double bilayers by atomic force microscopy, Biophys. J. 83 (5) (2002) 2625–2633.
[41] P.W. van Dijck, A.J. Kaper, H.A. Oonk, J. de Gier, Miscibility properties of binary phosphatidylcholine mixtures. A calorimetric study, Biochim. Biophys. Acta 470 (1) (1977) 58–69.
[42] J. Bernardino de la Serna, J. Perez-Gil, A.C. Simonsen, L.A. Bagatolli, Cholesterol rules: direct observation of the coexistence of two fluid phases in native pulmonary surfactant membranes at physiological temperatures, J. Biol. Chem. 279 (39) (2004) 40715–40722.
[43] F.M. Goni, A. Alonso, L.A. Bagatolli, R.E. Brown, D. Marsh, M. Prieto, J.L. Thewalt, Phase diagrams of lipid mixtures relevant to the study of membrane rafts, Biochim. Biophys. Acta 1781 (11-12) (2008) 665–684.
[44] L. Rodriguez Arriaga, J. Ipsen, A. Garcia, S. Härtel, F. Monroy, L.A. Bagatolli, Lipid domains in giant vesicles composed of ternary lipid mixtures containing cholesterol and their relationship with thermodynamic phases. 2009 Biophysical Society Meeting Abstracts, Biophys. J. 96 (3) (2009) 161a.